Journal of Hydraulic Research

ISSN: 0022-1686 (Print) 1814-2079 (Online) Journal homepage: http://www.tandfonline.com/loi/tjhr20

Simulations of granular bed erosion due to a mildly turbulent shear flow

Jos J. Derksen

To cite this article: Jos J. Derksen (2015) Simulations of granular bed erosion due to a mildly turbulent shear flow, Journal of Hydraulic Research, 53:5, 622-632, DOI: 10.1080/00221686.2015.1077354

To link to this article: http://dx.doi.org/10.1080/00221686.2015.1077354

Journal of Hydraulic Research Vol. 53, No. 5 (2015), pp. 622–632
http://dx.doi.org/10.1080/00221686.2015.1077354

Research paper

Simulations of granular bed erosion due to a mildly turbulent shear flow

JOS J. DERKSEN, Professor, *Chemical Engineering, Delft University of Technology, Delft, The Netherlands; School of Engineering, University of Aberdeen, Aberdeen, UK*
Email: jderksen@abdn.ac.uk

ABSTRACT
Three-dimensional, time-dependent simulations of the erosion of a granular bed consisting of monosized, non-cohesive spherical particles are reported. The simulations fully resolve the turbulence and the flow around each of the spheres (particle-resolved, direct simulations). The erosion is due to the turbulent flow of a Newtonian liquid in a planar channel with a Reynolds number based on wall shear velocity and channel height of 168. The main control parameter in the simulations is the Shields number that was varied between 0.03 and 0.60. The simulations were performed by means of a lattice Boltzmann scheme supplemented with an immersed boundary method to impose no-slip conditions at the particle surfaces. The results show the impact of the Shields number on the mobility of the particles at the top and above the bed. They also show a strong coupling between solids motion and the strength of the turbulent fluctuations in the liquid. Specifically, directly above the bed the particles significantly enhance turbulence at the lower end of the Shields number range investigated.

Keywords: Direct numerical simulations; erosion processes; lattice Boltzmann methods; particle-laden flows; turbulence–sediment interactions

1 Introduction

Erosion of granular beds by a shear flow is very common in natural and engineered systems; river and sea beds (Parker, 1990), pipelines transporting slurries (Gillies & Shook, 2000), dredging applications (Miedema, 2012), and solids suspension processes in mixing tanks (Ayranci et al., 2012) are only a few examples. All of these systems show a strongly inhomogeneous solids distribution and, as a result, an inhomogeneous flow pattern with relatively low velocities in and closely above the bed, and much higher velocities far away from the bed. The dynamics of granular bed erosion are, at least for non-cohesive particles, mainly the result of a competition between net gravity establishing the bed, and hydrodynamic forces that cause solid particles to move and get entrained by the flow. This competition is reflected in the dimensionless Shields number θ (Shields, 1936), which is the ratio of shear stress at the bed surface τ to the net gravity: $\theta \equiv \tau/g(\rho_p - \rho)d_p$ (where ρ and ρ_p are the liquid and solids density respectively, d_p is some average particle size, and g is gravitational acceleration). The Shields number is widely used to characterize sheared granular beds (Buffington & Montgomery, 1997; Ouriemi, Aussillous, Medale, Peysson, & Guazzelli, 2007). Other dimensionless groups, such as Reynolds numbers (overall and particle-based), and aspect ratios, influence the erosion process. It is expected that the characteristics of the flow above the bed play an important role and, as an example, it will make a difference if the flow shearing the bed is laminar or turbulent, a feature that is unaccounted for in the Shields number.

There is an extensive literature of experimental work on sheared granular beds. A review is beyond the scope of this paper (see e.g. Buffington & Montgomery, 1997). What strikes is the enormous variety of experimental systems and methods. They can be found almost anywhere on the spectrum between highly controlled, small-scale systems with laminar flow over monosized, spherical particles (e.g. Charru, Mouilleron, & Eiff, 2004; Lobkovsky, Orpe, Molloy, Kudrolli, & Rothman, 2008; Mouilleron, Charru, & Eiff, 2009) and large-scale turbulent systems directly reflecting the complexity of practically relevant processes (Uijttewaal, 2014).

Numerical simulations of granular bed erosion are valuable as they can quickly and cheaply scan solid–liquid flow conditions without the need for experiments. Simulations are also used for designing and scaling up (industrial) processes involving erosion (De Wit, Talmon, & Van Rhee, 2014). In addition, numerical simulations have a role to play in the detailed analysis

Received 18 January 2015; accepted 24 July 2015/Open for discussion until 30 April 2016.

ISSN 0022-1686 print/ISSN 1814-2079 online
http://www.tandfonline.com

of the complex phenomena of granular bed erosion by revealing the nature and relative strength of the liquid–solid and particle–particle interactions. The details of these interactions influence a wide spectrum of length scales (from grain size to system size) and time scales. To provide information about small-scale interactions, the present author recently reported simulations of granular bed erosion by a laminar shear flow where most of the fluid and solids dynamics were resolved explicitly (Derksen, 2011). The flow in and over a bed of monosized, non-cohesive spherical particles was simulated down to the level of imposing no-slip conditions at the individual spherical surfaces and thus resolving the liquid flow around each particle. The resulting hydrodynamic forces and torques on each sphere were subsequently used to integrate their translational and rotation dynamics, thereby providing updated no-slip conditions for the liquid and so creating an intimate coupling between liquid flow and solids motion. With these simulations it was possible to reproduce experimental observations of incipient motion in granular beds (Ouriemi et al., 2007) if adequate choices regarding friction and lubrication forces between closely spaced and touching grains were made. Similar particle-resolved simulations were also reported three years later by Kidanemariam and Uhlmann (2014a).

Extensions towards highly resolved simulations of turbulent flows over rough surfaces and of granular bed erosion are very relevant and are emerging in the literature (Breugem & Boersma, 2005; Chan-Braun, García-Villalba, & Uhlmann, 2011; Kidanemariam & Uhlmann 2014b; Vowinckel, Kempe, & Fröhlich, 2014). Topics studied through simulation include the extent to which the structure of turbulent boundary layers changes over rough walls and how friction increases forces and torques on particles and entrainment mechanisms.

In the present paper, the computational methodology as developed in Derksen (2011) was used to study larger scale systems with a mildly turbulent flow eroding the bed. The goal of this paper is to highlight the feasibility of such simulations and, more importantly, to show the strong interactions between levels of (turbulent) fluctuations and the dynamics of the solids in the close vicinity of the bed's surface and how these depend on the Shields number. It should be noted that the systems studied, although they are turbulent, are of small scale; in general they are too small to capture phenomena such as dune or ripple formation (experimental: Doucette & O'Donoghue, 2006; computational: Kidanemariam & Uhlmann, 2014b). In recent work, Vowinckel et al. (2014) report on turbulent simulations in open channels with resolved particles. By using structured beds and conditions such that very few particles entrain, they are able to study individual erosion events in detail. In the present paper, entrainment rates are usually much higher and the main interest is how the collective dynamics of solids and fluid is influenced by the interaction between particle behaviour (erosion, saltation and suspension) and near-bed turbulence.

The rest of the paper is structured as follows. In Section 2 the flow system is defined and characterized in terms of dimensionless numbers. In Section 3 the computational methodology is summarized; for a detailed description refer to Derksen (2011). In presenting the results (Section 4), firstly single-phase turbulence over a smooth wall and over a fixed particle bed is characterized. These flows serve as base cases for comparison with two-phase (solid–liquid) flow results. We then show how particle motion perturbs the turbulent boundary layer and, vice versa, turbulence alters the granular bed. The final section (Section 5) summarizes the main findings and conclusions from this work and provides an outlook to future work.

2 Flow system

The flow configuration, along with a Cartesian coordinate system that will be used throughout this paper, is sketched in Fig. 1. It is a channel with a horizontally placed flat wall of dimensions $L \times W$ that supports a granular bed of monosized solid spheres with radius a and density ρ_p. The typical height of the granular bed is $h \approx 10a$. A monolayer of spheres with surface fraction $\sigma \equiv n\pi a^2 \approx 0.7$ (with n the number of spheres per surface area) on the bottom wall is immobile. The rest of the spheres are allowed to move (except in one "fixed-bed" simulation in which all spheres are immobile). The granular bed is created by first placing the fixed monolayer on the bottom wall and subsequently randomly dropping spheres (through a vacuum) on the bed where they collide inelastically (restitution coefficient $e = 0.8$) with other spheres. This eventually creates a random, loosely packed bed of spheres. The space above the bed extends to $z = H$.

After the bed has been formed, the entire volume not occupied by the spheres is filled with a Newtonian liquid with kinematic viscosity ν and density ρ. A body force f in

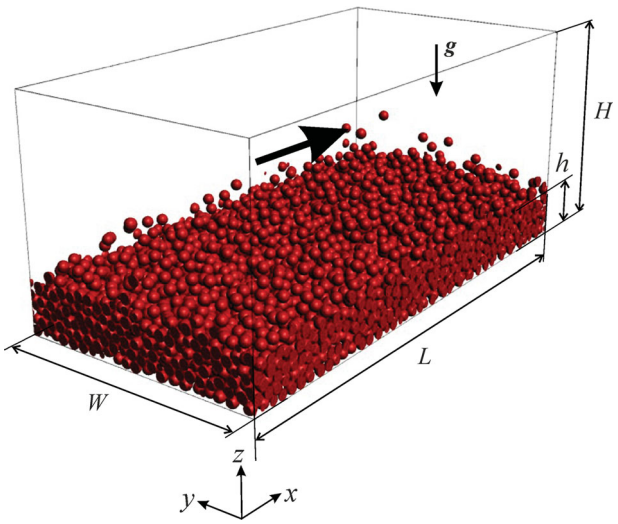

Figure 1 Flow geometry and coordinate system. Periodic boundary conditions apply in x and y directions. The bottom wall ($z = 0$) is a no slip-wall with a monolayer of spheres attached to it. The top boundary ($z = H$) has a free-slip condition. The particles are monosized spheres with radius a. Gravity acts in the negative z-direction; main flow is in the x-direction

x-direction (f is a force per unit volume acting on the liquid, it can be interpreted as an overall pressure gradient in x-direction) generates a mildly turbulent flow over the granular bed. At $z = H$ a no-penetration and free-slip boundary condition applies; the boundary conditions in x and y-direction are periodic; and no-slip is imposed on all solid surfaces.

Four independent dimensionless numbers determine the flow system defined above. These are (1) a channel-based Reynolds number $\mathsf{R}_\tau \equiv (H-h)u_\tau/\nu$ with $u_\tau = \sqrt{f\,(H-h)/\rho}$ the wall shear velocity; (2) the Shields number $\theta = (H-h)f\,/[2ag(\rho_p-\rho)]$ (note that the shear stress at the bed surface relates to the body force f through an overall force balance in streamwise direction: $\tau = f\,(H-h)$); (3) the density ratio ρ_p/ρ; and (4) the ratio of particle radius and channel height a/H. As we will see below, other dimensionless numbers such as a Stokes number or particle-based Reynolds numbers can be expressed in terms of these four independent dimensionless groups. Three of the four groups (R_τ, ρ_p/ρ, and a/H) have fixed values in this study. These values were chosen for a variety of reasons: availability of reference data (R_τ), earlier results for laminar flow (ρ_p/ρ) and computational feasibility (a/H). The Shields number has been varied over an interval that includes the Shields number of incipient bed motion (the critical Shields number θ_c) at the actual Reynolds number as experimentally determined for laminar flow ($\theta_c \approx 0.05$) (Ouriemi et al., 2007) as well as under turbulent conditions (θ_c in the range 0.04–0.05) (Shields, 1936).

The flow Reynolds number has the fixed value of $\mathsf{R}_\tau = 168$. This is close to $\mathsf{R}_\tau = 180$ which was applied in the seminal paper by Kim, Moin, and Moser (1987) on direct numerical simulations of the flow between two parallel plates, and $\mathsf{R}_\tau = 171$ as simulated by Lam and Banerjee (1992) for the case, comparable to this paper, of a planar channel with one no-slip and one free-slip boundary. In the latter paper the length and width of the channel were 2π and π times its height respectively; in our paper $L = 3(H-h)$ and $W = 1.5(H-h)$ which implies significantly smaller aspect ratios. This choice was made to limit the number of particles in the simulations, thus reducing the computational cost. By means of a simulation without particles it will be shown that at least the first and second order statistics of the turbulent flow in our channel agree with those obtained by Lam and Banerjee (1992). For a channel bounded by two parallel solid walls, Jimenez and Moin (1991) found a minimum channel width and length of 100 and 250–350 wall units respectively to sustain turbulence. The channel in the current study has $W^+ \approx 250$ and $L^+ \approx 500$, i.e. well beyond the minimum dimensions identified by Jimenez and Moin (1991).

The sphere radius $a = H/40$; in terms of wall units, $a^+ \equiv u_\tau a/\nu = 5.6$. The density ratio $\rho_p/\rho = 4.0$ throughout this paper in line with our previous work on laminar bed erosion (Derksen 2011). The expression for the Shields number is $\theta = (H-h)f\,/[2ag(\rho_p-\rho)]$. Gravity acts in the negative z-direction (see Fig. 1): $\mathbf{g} = -g\mathbf{e_z}$. The Stokes number based on particle diameter and wall shear velocity $\mathsf{St} \equiv \frac{\rho_p}{18\rho}\frac{2au_\tau}{\nu} = \frac{1}{18}\frac{\rho_p}{\rho}\frac{2a}{H}\mathsf{R}_\tau$ has a value of 2.5 throughout this paper. This Stokes number of order one signifies the interesting case of inertial particles that are at the same time sensitive to their direct hydrodynamic environment.

In this paper the focus is on the impact of the Shields number on liquid and particle behaviour without interfering effects from the variation of other dimensionless numbers. For that reason, the Shields number has been varied while keeping the Reynolds number R_τ constant. A unique feature of simulations is that this can be achieved easily by varying g, which is obviously different from how it might be done in experiments.

3 Modelling approach

We perform direct simulations with resolved particles. The computational approach is the same as used by Derksen (2011) for erosion of granular beds by laminar shear flows. The lattice Boltzmann (LB) method (Aidun & Clausen, 2010; Chen & Doolen, 1998; Succi, 2001) is used as the flow solver. It operates on a uniform, cubic lattice with lattice spacing Δ. An immersed boundary method (IBM) imposes no-slip conditions on the surfaces of the particles by locally forcing the liquid to the same velocity as the solid surface (Ten Cate, Nieuwstad, Derksen, & Van den Akker, 2002). The IBM includes calibration of the sphere size which is needed as a consequence of representing a curved surface on a cubic grid (Ladd, 1994; Ten Cate et al., 2002). Per-particle integration of these forces over their surface provides the hydrodynamic force and torque on each particle. The particles move (translate and rotate) under the influence of these hydrodynamic forces and torques, net gravity, and collisions.

A hybrid time-step/event-driven algorithm integrates particle velocities and positions. Each time step, first the flow field, and thus also the force and torque on each particle, is updated by means of the LB method. Then velocities (translational and angular) are updated as a result of the hydrodynamic forces and torques, and gravity. For stability reasons we use mixed-derivative integration (Shardt & Derksen, 2012) for this. Subsequently the particles move ballistically for the duration of the time step, where they potentially undergo hard-sphere collisions according to a model (Yamamoto, Potthoff, Tanaka, Kajishima, & Tsuji, 2001) that has two parameters: a restitution coefficient e and a friction coefficient μ. At the end of this process the next time step can begin. It should be noted that the time step in the simulations is very small as instigated by incompressibility constraints of the LB method (e.g. Succi, 2001): the time resolution is such that $\Delta t \approx a/(2.1 \times 10^3 u_\tau)$. As we will see, the maximum velocity in the flow is of the order of $20u_\tau$ so that a particle in "free-flight" would maximally move over a distance of $20u_\tau\Delta t \approx 10^{-2}a$ during one time step. The hard-sphere collision algorithm is restricted to binary collisions and does not consider enduring contacts between the spheres. This implies continuous motion of all spheres with only minute

motion deeper in the bed where also many and very weak collisions occur. These collisions slow down the simulations to some extent, specifically at the low end of the Shields number range, i.e. under high g conditions. The reason for using the hard-sphere algorithm is its good past performance (Derksen, 2011) in recovering critical erosion conditions under laminar shear flow.

As described above, hydrodynamic forces on the particles directly follow from applying the immersed boundary method in the context of an LB flow solver. The latter operates on a fixed, uniform grid. In dense suspensions of colliding particles inevitably particle surfaces come closer to one another than the grid spacing, making the flow in between the particles underresolved in the simulations. To compensate for this, the resolved hydrodynamic forces are supplemented by (unresolved) lubrication forces, which follow from analytical solutions of the creeping flow in the narrow gap between two spherical surfaces that move relative to one another (Kim & Karrila, 1991). The approach as proposed by Nguyen and Ladd (2002) in the context of LB simulations has been implemented and applied in the current work, as it also was in our previous works.

In addition to the Reynolds number, Shields number, density ratio, and aspect ratios $(L/H, W/H, a/H, h/a)$ defined in the previous section, extra dimensionless parameters enter as a result of physical modelling and the use of numerical methods. The hard-sphere collision model has two parameters: the restitution coefficient has been set to $e = 1$, the friction coefficient to $\mu = 0.1$. For liquid systems, the specific choice of restitution coefficient is not that sensitive as most energy dissipation takes place in the liquid phase, not in collisions (Derksen & Sundaresan, 2007). The choice for $\mu = 0.1$ is based on our experience with erosion in laminar flow (Derksen, 2011) where it was demonstrated that some level of friction is needed to allow particles to roll over one another, which is an important erosion mechanism, specifically under conditions near incipient motion. It also was observed in Derksen (2011) that the specific level of friction had limited effect on the outcome of the simulations, i.e. results for $\mu = 0.10$ and $\mu = 0.25$ only showed marginal differences.

The spatial resolution of the simulations has been set to $a/\Delta = 6$ (with Δ the lattice spacing). In many of our previous papers the effect of resolution has been assessed through grid refinement studies (most recently in Derksen, 2014), and comparisons with experimental data (Ten Cate et al., 2002). They consistently show that as long as Reynolds numbers based on slip velocity and particle diameter do not exceed 30, grid effects are marginal. The temporal resolution was such that the dimensionless time step $\Delta t u_\tau/a = 4.67 \times 10^{-4}$.

Finally, the lubrication force model needs two parameters (Derksen & Sundaresan, 2007): the distance between two solid surfaces below which the lubrication force becomes active (δ), and the distance below which the lubrication force saturates (ε). These distances were chosen the same as in Derksen (2011): $\delta/a = 0.2$ and $\varepsilon/a = 2 \times 10^{-4}$.

4 Results

4.1 *Single-phase turbulent channel flow*

Since the horizontal dimensions L and W are relatively small, it first needs to be established that they are sufficiently large to allow the generation of a representative turbulent flow. For that reason we performed one simulation without particles and a channel height $H' \equiv H - h$. In another single-phase simulation we placed an immobile particle bed of depth h on the lower plate (which was the same particle bed we used as the starting configuration for the simulations with mobile particles). In both single phase cases a turbulent flow develops as can be seen from the yz liquid velocity vector fields (symbol **u**) in a cross section of the flow in Fig. 2. In the lower panel, which represents the flow over the immobile bed, it is interesting to note that the small-scale flow structures at the surface of the bed quickly disappear higher up in the channel. There the flow very much resembles the flow over the smooth bottom wall.

Wall-normal profiles of first and second order statistics have been collected in the conventional way (Kim et al., 1987) by averaging over the two homogeneous directions (x and y) and over time. For the smooth channel the results are presented in Fig. 3; these results are collected over a time span of $tu_\tau/a = 190$. The left panel shows the streamwise velocity profile in

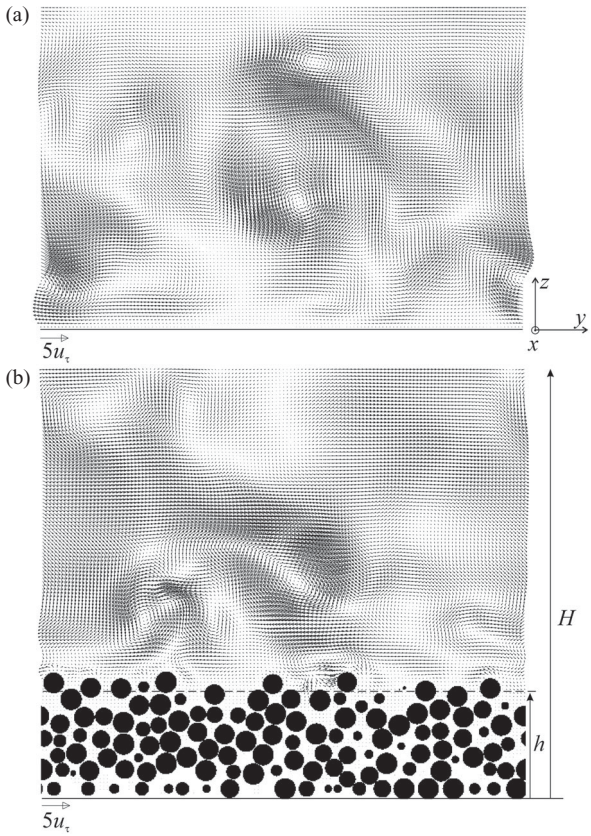

Figure 2 Velocity vector fields in lateral (yz) cross sections. (a) Flow through a channel without particles. (b) Flow over a bed of fixed particles. Instantaneous realizations

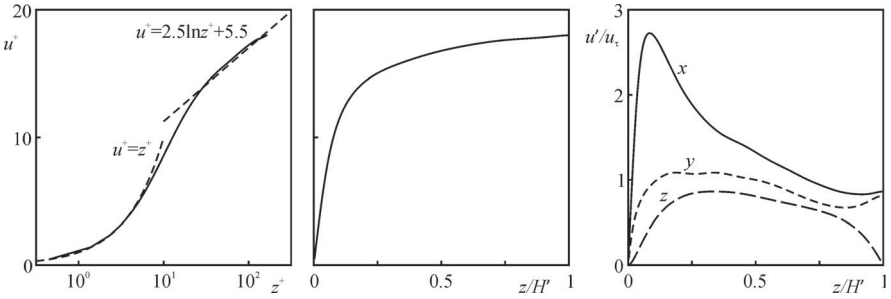

Figure 3 Average wall-normal velocity profiles for a channel without particles. Left: average velocity in terms of wall units; middle: average velocity; right: velocity fluctuations in the three coordinate directions

wall units $u^+ \equiv \overline{\langle u \rangle}/u_\tau$ (hooked brackets for spatial average, overbar for time average) and $z^+ \equiv zu_\tau/\nu$. With z^+ on a logarithmic scale, the viscous sublayer and the logarithmic layer (Hinze, 1975) can be clearly identified with good agreement with the results due to Lam and Banerjee (1992). The middle panel contains the same data as the left panel but now on linear axes. It shows the familiar shape of the average streamwise velocity of a turbulent flow with a relatively flat profile in the region away from the wall due to the strong lateral mixing as a result of turbulence. The root mean square velocity profiles $\left(u' \equiv \sqrt{\overline{\langle u^2 \rangle} - \overline{\langle u \rangle}^2}\right)$ are given in the right panel and also agree well with those reported by Lam and Banerjee (1992). The streamwise fluctuations peak at $z/H = 0.085$ to a level $u'/u_\tau = 2.72$. The velocity fluctuations in z-direction are zero at $z = H'$ due to non-penetrable boundary there.

A similar dataset but for the flow over a fixed bed of spheres is given in Fig. 4. In addition, the solids volume fraction (ϕ) profile is presented. The coherent wiggles in the ϕ profile are due to the ordering effect the flat plate supporting the bed has on the particle configuration and the fact that resolution of the profile is finer than the particle size. The five (to six) peaks in the profile relate to five (to six) layers of particles the bed consists of (bed height $h \approx 10a$). The streamwise average velocity inside the particle bed is virtually absent. Above the bed, there is great similarity with the flow over the smooth wall. In the average streamwise velocity profile, the viscous sublayer and the logarithmic layer can still be identified. Compared to the smooth wall there is a velocity deficit of approximately $\Delta u^+ \approx 2$ (Jiménez, 2004). As explained by Hinze (1975), such a deficit is a function of ku_τ/ν with k the length scale of the wall roughness. If we choose $k \approx 2a$ (e.g. based on the cross sectional view through the bed as shown in Fig. 2, lower panel) then $ku_\tau/\nu \approx 10$. Data reprinted in Hinze (1975, fig. 7–16) then show that $\Delta u^+ \approx 2$ falls well within what has been observed experimentally. The velocity fluctuation profiles above the rough wall are very similar to those above the smooth wall.

In Fig. 5, impressions are shown to demonstrate how the flow makes the transition of being clearly perturbed by the presence of the particles at the upper levels of the bed to a flow akin to the flow over a smooth wall higher up in the

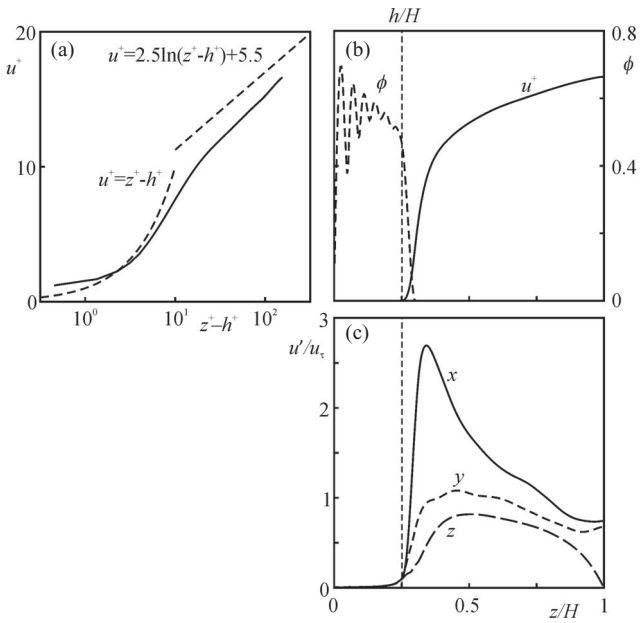

Figure 4 Average wall-normal profiles for the flow over a fixed bed of particles. (a) Average velocity in terms of wall units; (b) average velocity and solids volume fraction ϕ; (c) velocity fluctuations in the three coordinate directions. The parameter h is an estimate of the bed height

channel. This is done by means of instantaneous contours of the z-velocity at three z-levels. The left panels are for the smooth wall; the right panels for the rough wall. For $z^+ = 5.1$ above the smooth wall, next to vertical velocity contours also horizontal velocity vectors are given and the correlation between low streamwise speed regions and upward velocity, and high speed streaks and downward velocity can be clearly observed. Higher above the smooth wall (at $z^+ = 16.3$, and 21.9) the spanwise length scales get larger and vertical velocities get more pronounced. Over the rough wall at $z^+ - h^+ = 5.1$ the picture is completely different with upward and downward velocity dominated by the presence of the spheres. At $z^+ - h^+ = 16.3$ the effects of individual spheres can still be identified but at the same time the pattern much more resembles the flow over the smooth wall at the same level (in plus units). Finally, at $z^+ - h^+ = 21.9$ the flows over rough and smooth wall are qualitatively very similar.

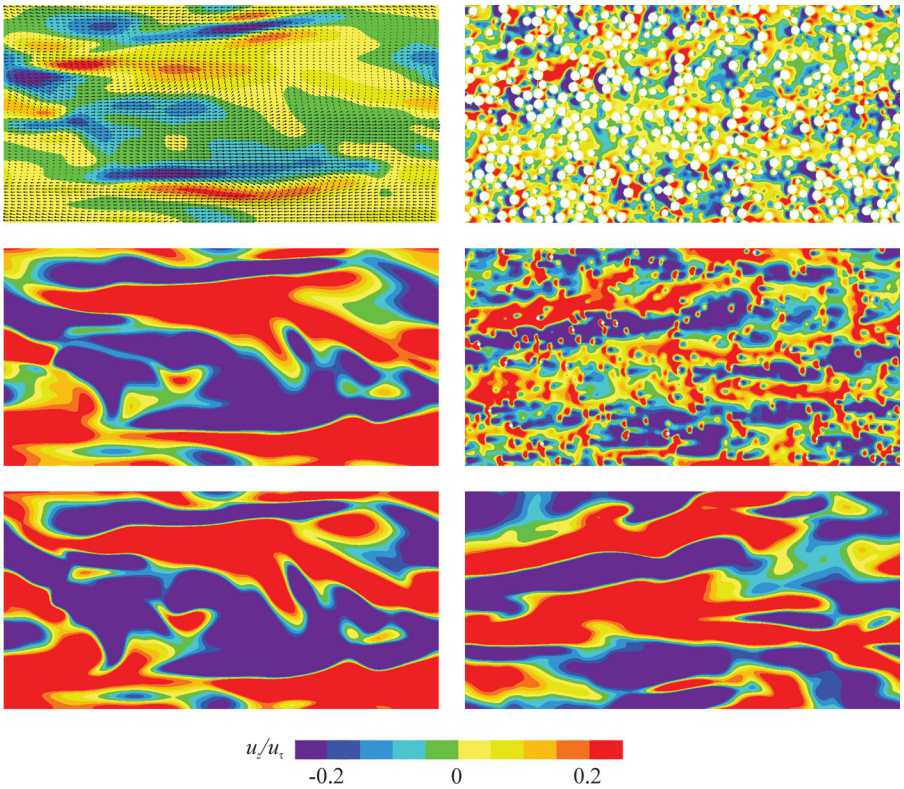

Figure 5 Contours of instantaneous realizations of wall-normal velocity u_z in xy planes. Left column: flow in channel with smooth bottom wall at (from top to bottom) $z^+ = 5.1, 16.3,$ and 21.9, respectively. In the upper left panel velocity vectors (with x and y component $u_x/u_\tau - z^+$ and u_y/u_τ respectively) have been superimposed. Right column: flow over a fixed particle bed at $z^+ - h^+ = 5.1, 16.3,$ and 21.9

4.2 *Solid particle motion*

Simulations with mobile spheres were started from the fully developed fixed bed simulation as described above. At moment $t = 0$ we simply switched from immobile to mobile particles. The range of Shields numbers considered was from $\theta = 0.03$ to $\theta = 0.60$.

A qualitative view of the impact of the Shields number on particle motion and liquid flow is given in Fig. 6. From high to low θ, the level of solids motion strongly decreases. At the same time the liquid velocity magnitude seems to get somewhat smaller for higher θ. For the lowest Shields number simulated in this paper ($\theta = 0.03$) we do see persistent motion of a few spheres, indicating that 0.03 is still above the critical Shields number associated with incipient motion of solids. Ouriemi et al. (2007) have collected data for the critical Shields number (θ_c) for *laminar* shear flow as a function of a particle-based Reynolds number ($\mathsf{R} = \dot{\gamma} 4a^2/\nu$) with $\dot{\gamma}$ the shear rate. If we substitute $\dot{\gamma} = \tau/(\rho\nu)$, then $\mathsf{R} = 120$ under the current simulation conditions. Then according to Ouriemi et al. (2007), $\theta_c \approx 0.05$, and the tentative conclusion is that turbulence is responsible for a reduction in θ_c (Vollmer & Kleinhans, 2007). The original work of Shields (1936) does deal with turbulent flow and reports a θ_c in the range 0.04–0.05 at a particle-based Reynolds number $\mathsf{R} = 120$ (see *Abbildung* 6 in Shields, 1936). Given that Shields worked with non-spherical particles (having a narrow size distribution) that are harder to mobilize than spheres, $\theta_c < 0.03$, as found in the current study, seems physically realistic.

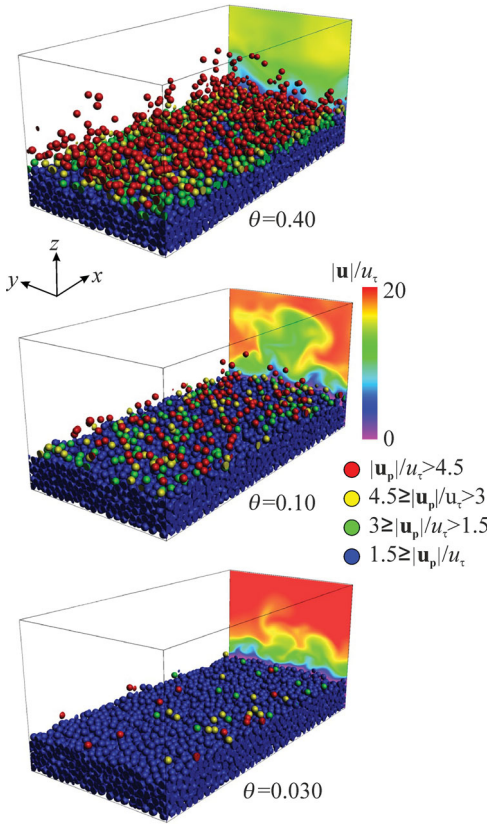

Figure 6 Single realizations of erosion simulations at three different Shields numbers. Particles have been coloured by their speed $|\mathbf{u_p}|$ as indicated. The contours in the back plane ($x = L$) denote the liquid velocity magnitude

It appeared to be a lengthy process to bring the solid–liquid flows to a steady state, specifically for the higher Shields numbers. Steady state was monitored in terms of time series of the average streamwise velocity of the mobile particles $\langle u_p \rangle$ (note that part of the particles, those on the bottom plate, are immobile). Figure 7 contains examples of such time series. The overshoot, most clearly visible for $\theta = 0.60$, is the result of the two-way coupling between solid and liquid. With initially many particles entraining in the liquid for high Shields numbers, the mean flow and the turbulent fluctuations attenuate, leading to partial re-deposition of the entrained particles. This evolves until a dynamic balance is struck between entrainment and deposition. This evolution takes a time period of order $t = 10H/u_\tau$ for $\theta = 0.60$. With a free stream velocity of order $20u_\tau$ and a channel length of $L = 2.25H$ it means that during this time period a liquid parcel in the free stream traversed almost 90 channel lengths. Fortunately, the time to steady state is much faster for lower Shields numbers (Fig. 7) because entrainment of particles then is much weaker.

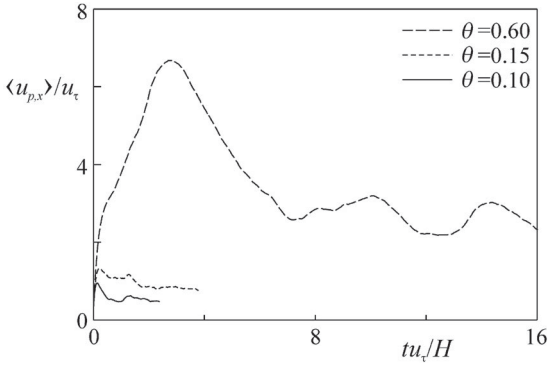

Figure 7 Average streamwise velocity of the particles as a function of time for three values of the Shields number

Inspired by the experimental work due to Ramesh, Kothyari, and Murugesan (2011), traces of particles are shown in Fig. 8. For the three Shields numbers that were selected for this figure we randomly took seven particles and plotted their location in xz and yz plane with a time interval of $t = 0.093a/u_\tau$. A number of deposition and entrainment events can be identified in these time traces. In the xz-views the effect of the Shields number is very obvious. The particles get higher up in the flow and (thus) move faster for the higher Shields number. The lateral displacements (the yz-views) qualitatively show an interesting trend with the strongest lateral motion for the intermediate Shields number of $\theta = 0.15$. At the low Shields number of $\theta = 0.075$ particle displacement is weak in any direction; as we will see later, damping of liquid flow turbulence by the particles weakens lateral particle dispersion which explains less lateral motion

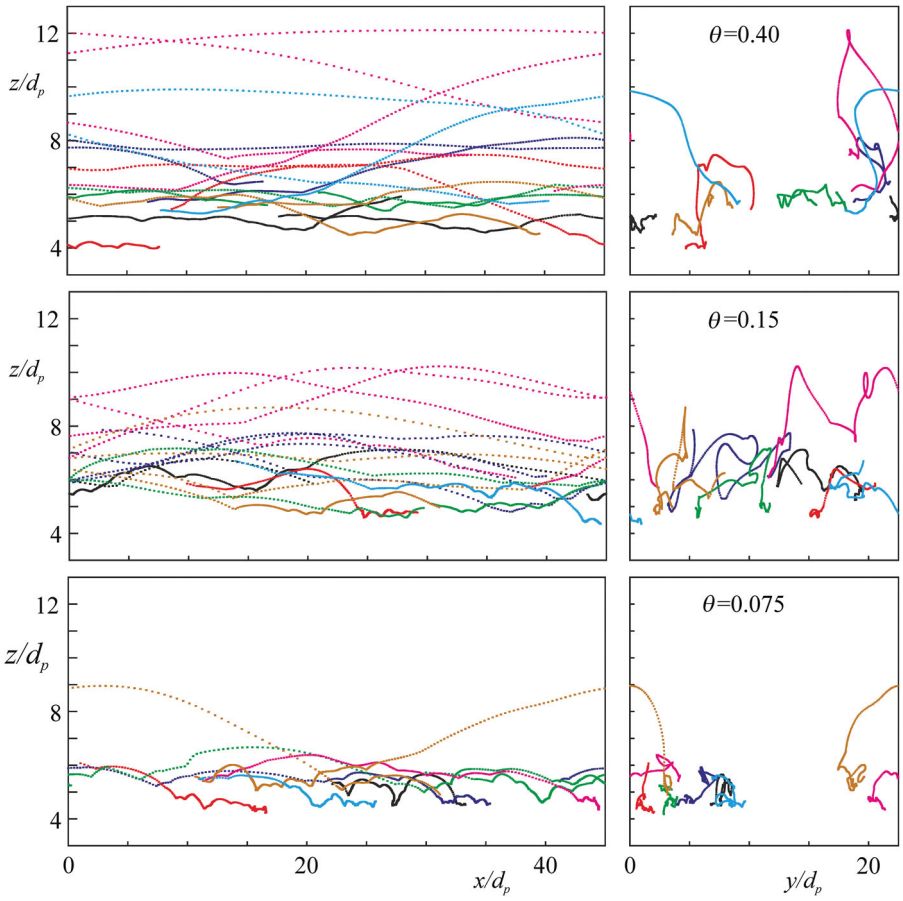

Figure 8 Particle trajectories over a timespan $36.8a/u_\tau$ in xz (left) and yz (right) views for three Shields numbers. Per Shields number, seven trajectories (each with its own colour) are plotted. The seven particles were selected randomly

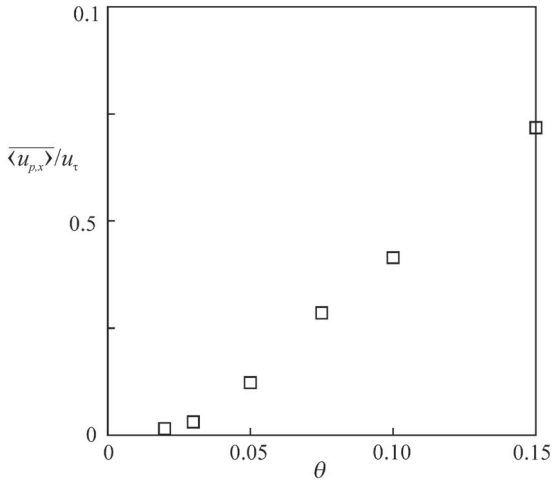

Figure 9 Time and volume average particle velocity in the streamwise direction as a function of the Shields number

for $\theta = 0.40$ compared to $\theta = 0.15$; turbulence attenuation is largely restricted to the higher Shields numbers ($\theta \geq 0.40$ in this study) investigated.

Results on particle motion for $\theta \leq 0.15$ have been summarized in terms of the steady-state, time-averaged, volume average velocity of the mobile spheres in Fig. 9. As indicated before, $\theta = 0.03$ was the lowest Shields number simulated. For that case we still see a non-negligible particle flux in and over the bed. A cautious extrapolation of the data points in Fig. 9 indicates a critical Shields number in the range $0.015 \leq \theta_c \leq 0.025$.

4.3 *Interaction between flow and solids motion*

An attempt to quantify the way liquid flow and solids motion interact is given in Fig. 10. Average quantities are in the left column of panels; fluctuation levels in the right column. The solids velocity profiles do not extend over the full z/H range. Beyond the z-location where the profiles end, no particle has been detected in the entire time window over which was averaged. The wiggles near the end of the profiles are thus due to poor (particle) statistics.

The level of entrainment is clear from the solids volume fraction profiles that extend higher up for higher θ. However, at least for $\theta \leq 0.15$, the particle bed retains the five-peak structure in the ϕ-profile which indicates that there is a more-or-less static bed of particles of height $h \approx 10a$; something which is qualitatively confirmed in Fig. 6. The average solids streamwise velocity slightly lags the liquid's streamwise velocity, a common feature in turbulent, particle-laden horizontal flows (Kiger & Pan, 2002). This lag is estimated as $u^+ = 4$ at most (for $\theta = 0.10$). This estimate, which is larger than maximum velocity fluctuation levels of $u'/u_\tau \approx 3$, we use to assess the maximum Reynolds number based on slip velocity and sphere diameter: It is $\mathsf{R}_{\mathsf{slp}} \equiv 2a|\mathbf{u} - \mathbf{u_p}|/\nu = 45$. As was indicated above, the spatial resolution of the spheres on the grid ($a/\Delta = 6$) has been validated up to $\mathsf{R}_{\mathsf{slp}} \approx 30$ (Ten Cate et al., 2002)

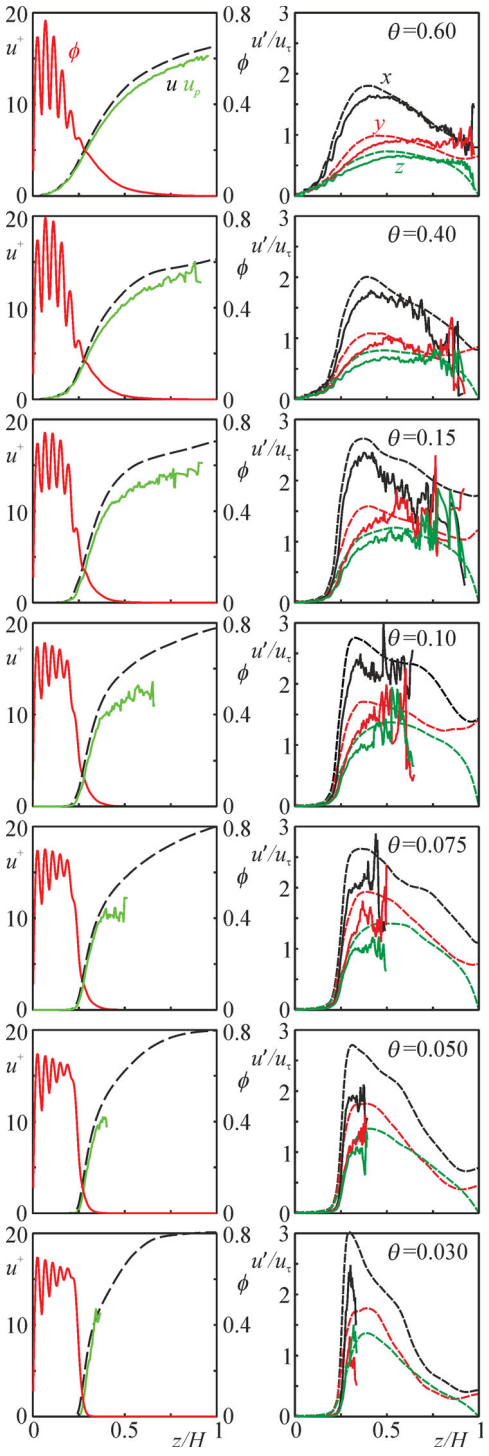

Figure 10 Left column: average streamwise liquid and particle velocity and solids volume fraction profiles. Right column: liquid (dashed curves) and particle (solid curves) velocity fluctuation profiles. Shields numbers (indicated) decrease from top to bottom

so that we are fairly confident of having performed sufficiently resolved simulations.

The solid and liquid velocity fluctuation levels show a very interesting trend with the Shields number. At the higher Shields numbers ($\theta = 0.60$ and 0.40) liquid velocity fluctuations are clearly damped over the entire height of the channel (compared to the liquid-only flow over the fixed particle

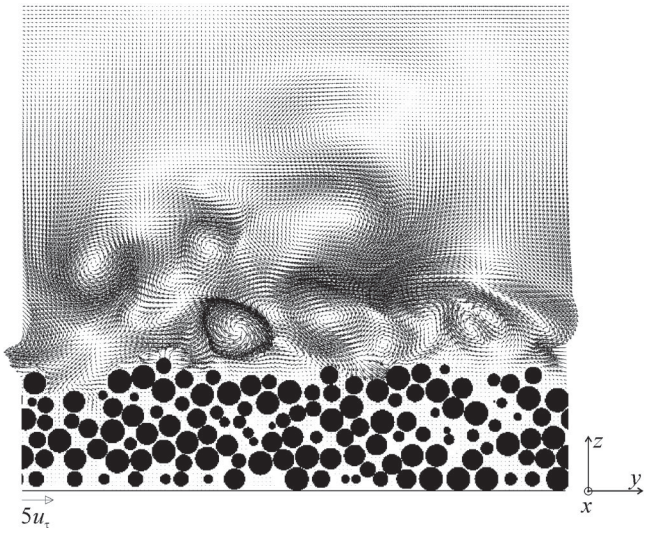

Figure 11 Velocity vector fields in lateral (yz) cross sections at $\theta = 0.03$. Instantaneous realization

bed). Such damping of turbulence by inertial particles has been reported before, notably in recent simulations by Lucci, Ferrante, and Elghobashi (2010) on inertial particles in homogeneous isotropic turbulence.

At lower Shields numbers ($\theta \leq 0.15$ in Fig. 10), however, liquid velocity fluctuation levels increase and can get significantly higher than levels in the single-phase flow over the fixed bed. This effect we attribute to limited numbers of entrained particles "stirring" the liquid. As can be seen, the effect of enhanced liquid velocity fluctuations is localized to where particles are present and slightly higher up (up to a vertical distance of approximately $5a$). This effect is illustrated for $\theta = 0.03$ in Fig. 11 in terms of liquid velocity vectors in a yz-plane. It shows a very inhomogeneous flow with turbulent structures of a size of a few sphere diameters directly above the particle bed, and a much smoother and weaker turbulence, comparable to the single-phase channel flows, higher up.

As a final observation in Fig. 10 we note that the solids velocity fluctuations are generally smaller than the liquid velocity fluctuation levels, which is a result of the inertial character of the particles ($\mathsf{St} = 2.5$) as also noted in experimental work (Kiger & Pan, 2002).

5 Summary and conclusions

We studied erosion of beds of spherical particles, all having the same size, by a mildly turbulent shear flow by means of particle-resolved simulations with an emphasis on the effect of the Shields number at a constant Reynolds number $\mathsf{R}_\tau = 168$. Viewed in perspective of the turbulent boundary layer, the particles have a significant size; their radius in wall units is $a^+ = 5.6$. Although the flow domain is relatively small (its length spans 45 particle diameters) it was large enough to sustain a turbulent flow.

The generation of turbulence was benchmarked against results from the literature. The single-phase flow over a smooth wall compared favourably with the results of Lam and Banerjee (1992); the flow over a fixed particle bed showed a velocity deficit as a result of wall roughness in line with experimental data on this topic (e.g. Hinze, 1975).

The simulations with mobile particles show, as expected, a very strong sensitivity with respect to the Shields number. Down to a Shields number of 0.03 there consistently remains a weak flux of particles at the surface of the bed. Extrapolation of the particle flux as a function of the Shields number towards zero flux indicates a critical Shields number in the range 0.015–0.025. This is factor of two to three lower than experimentally observed for laminar shear flow at the same particle-based Reynolds numbers. Turbulent fluctuations are likely the reason for enhanced particle motion and thus erosion (Shields 1936).

We observed an interesting interaction between turbulent liquid fluctuations and the extent of bed erosion. For strong erosion with many particles entrained by the liquid flow, liquid turbulence is damped significantly. With limited erosion, liquid turbulence is enhanced. Since this turbulence enhancement is limited to the heights (plus about two particle diameters) to which particles are entrained we explain this by the stirring effect of particles moving relative to the liquid.

There are at least three directions in which this research could be extended. Firstly, the analysis of the current flow systems could be extended to allow for a close inspection of the interaction between turbulent structures and the way particles get dislocated from and fall back in the granular bed.

Secondly, it would be very interesting to do dedicated experiments on similar, well-defined systems as studied numerically here. The focus of the experiments could be on the turbulence damping/enhancement transition and thus would need careful measurements of the liquid flow in the presence of particles; this could be done through optical techniques (particle image velocimetry, laser Doppler anemometry) combined with refractive index matching so that it would be possible to measure closely above and possibly within the bed.

Thirdly, the domain size in the simulations should be enlarged in order to arrive at scales where structures in the particle bed should become visible (Kidanemariam & Uhlmann, 2014b). This would not only be a way to further test and validate the numerical procedure, but also to enhance our understanding of structure formation in granular beds. Obviously, larger domains require larger computational power. Given, however, that the simulations reported here were performed in a sequential (i.e. single CPU) way, there are certainly possibilities for larger scale simulations through parallel computing.

Notation

a = spherical particle radius (m)
d_p = particle diameter (m)
e = restitution coefficient (–)

f = body force (N/m^3)
g = gravitational acceleration (m s^{-2})
H = domain height (m)
H' = height of channel without particles (m)
h = granular bed height (m)
k = surface roughness length scale (m)
L = domain length (m)
n = number of particles per surface area in (fixed) monolayer (m^{-2})
R = Reynolds number (–)
St = Stokes number (–)
$\mathbf{u}$ = fluid velocity (m s^{-1})
$\mathbf{u_p}$ = particle velocity (m s^{-1})
u' = root mean square velocity (m s^{-1})
u_τ = wall shear velocity (m s^{-1})
W = domain width (m)
x, y, z = Cartesian coordinates (m)
$\dot{\gamma}$ = shear rate (s^{-1})
Δ = lattice spacing (m)
Δt = time step (s)
δ, ε = lubrication force parameters (m)
θ, θ_c = Shields number, critical Shields number (–)
μ = friction coefficient (–)
ν = kinematic viscosity (m^2 s^{-1})
ρ, ρ_p = fluid and particle density (kg m^{-3})
σ = surface occupancy of (fixed) monolayer (–)
τ = shear stress, wall shear stress (Pa)
ϕ = solids volume fraction (–)

References

Aidun, C., & Clausen, J. (2010). Lattice-Boltzmann method for complex flows. *Annual Review of Fluid Mechanics*, *42*, 439–472.

Ayranci, I., Machado, M. B., Madej, A. M., Derksen, J. J., Nobes, D. S., & Kresta, S. M. (2012). Effect of geometry on the mechanisms for off-bottom solids suspension in a stirred tank. *Chemical Engineering Science*, *79*, 163–176.

Breugem, W. P., & Boersma, B. J. (2005). Direct numerical simulations of turbulent flow over a permeable wall using a direct and a continuum approach. *Physics of Fluids*, *17*, 025103-1-15.

Buffington, J. M., & Montgomery, D. R. (1997). A systematic analysis of eight decades of incipient motion studies, with special reference to gravel-bedded rivers. *Water Resources Research*, *33*, 1993–2029.

Chan-Braun, C., García-Villalba, M., & Uhlmann, M. (2011). Force and torque acting on particles in a transitionally rough open-channel flow. *Journal of Fluid Mechanics*, *684*, 441–474.

Charru, F., Mouilleron, H., & Eiff, O. (2004). Erosion and deposition of particles on a bed sheared by a viscous flow. *Journal of Fluid Mechanics*, *519*, 55–80.

Chen, S., & Doolen, G. D. (1998). Lattice–Boltzmann method for fluid flows. *Annual Review of Fluid Mechanics*, *30*, 329–364.

Derksen, J. J. (2011). Simulations of granular bed erosion due to laminar shear flow near the critical Shields number. *Physics of Fluids*, *23*, 113303-1-12.

Derksen, J. J. (2014). Simulations of hindered settling of flocculating spherical particles. *International Journal of Multiphase Flow*, *58*, 127–138.

Derksen, J. J., & Sundaresan S. (2007). Direct numerical simulations of dense suspensions: wave instabilities in liquid-fluidized beds. *Journal of Fluid Mechanics*, *587*, 303–336.

De Wit, L., Talmon, A. M., & Van Rhee, C. (2014). 3D CFD simulations of trailing suction hopper dredger plume mixing: Comparison with field measurements. *Marine Pollution Bulletin*, *88*, 34–46.

Doucette, J. S., & O'Donoghue, T. (2006). Response of sand ripples to change in oscillatory flow. *Sedimentology*, *53*, 581–596.

Gillies, R. G., & Shook, C. A. (2000). Modelling high concentration settling slurry flows. *Canadian Journal of Chemical Engineering*, *784*, 709–716.

Hinze, J. O. (1975). *Turbulence*. New York: McGraw-Hill.

Jimenez, J. (2004) Turbulent flows over rough walls. *Annual Review of Fluid Mechanics*, *36*, 173–196.

Jimenez, J., & Moin, P. (1991). The minimal flow unit in wall turbulence. *Journal of Fluid Mechanics*, *225*, 213–240.

Kidanemariam, A. G., & Uhlmann M. (2014a). Interface-resolved direct numerical simulation of the erosion of a sediment bed sheared by laminar channel flow. *International Journal of Multiphase Flow*, *67*, 174–188.

Kidanemariam, A. G., & Uhlmann, M. (2014b). Direct numerical simulation of pattern formation in subaqueous sediment. *Journal of Fluid Mechanics*, *750*, R2-1-13.

Kiger, K. T., & Pan, C. (2002). Suspension and turbulence modification effects of solid particulates on a horizontal turbulent channel flow. *Journal of Turbulence*, *3*, 019-1-21.

Kim, J., Moin, P., & Moser, R. (1987). Turbulence statistics in fully developed channel row at a low Reynolds number. *Journal of Fluid Mechanics*, *177*, 133–166.

Kim, S., & Karrila, S. J. (1991). *Microhydrodynamics: Principles and selected applications*. Boston: Butterworth-Heinemann.

Ladd, A. J. C. (1994). Numerical simulations of particle suspensions via a discretized Boltzmann equation. Part 2. Numerical results. *Journal of Fluid Mechanics*, *271*, 311–339.

Lam, K., & Banerjee, S. (1992). On the condition of streak formation in a bounded turbulent flow. *Physics of Fluids A*, *4*, 306–320.

Lobkovsky, A. E., Orpe, A. V., Molloy, R., Kudrolli, A., & Rothman, D. H. (2008). Erosion of a granular bed driven by laminar fluid flow. *Journal of Fluid Mechanics*, *605*, 47–58.

Lucci, F., Ferrante, A., & Elghobashi, S. (2010). Modulation of isotropic turbulence by particles of Taylor length-scale size. *Journal of Fluid Mechanics*, *650*, 5–55.

Miedema, S. A. (2012). Constructing the shields curve part a: fundamentals of the sliding, rolling and lifting mechanisms for the entrainment of particles. *Journal of Dredging Engineering*, *12*, 1–49.

Mouilleron, H., Charru, F., & Eiff, O. (2009). Inside the moving layer of a sheared granular bed. *Journal of Fluid Mechanics*, *628*, 229–239.

Nguyen, N.-Q., & Ladd, A. J. C. (2002). Lubrication corrections for lattice-Boltzmann simulations of particle suspensions. *Physical Review E*, *66*, 046708.

Ouriemi, M., Aussillous, P., Medale, M., Peysson, Y., & Guazzelli, E. (2007). Determination of the critical Shields number for particle erosion in laminar flow. *Physics of Fluids*, *19*, 061706-1-4.

Parker, G. (1990). Surface-based bed-load transport for gravel rivers. *Journal of Hydraulic Research*, *28*, 417–436.

Ramesh, B., Kothyari, U. C., & Murugesan K. (2011). Near-bed particle motion over transitionally-rough bed. *Journal of Hydraulic Research*, *49*, 757–765.

Shardt, O., & Derksen, J. J. (2012). Direct simulations of dense suspensions of non-spherical particles. *International Journal of Multiphase Flow*, *47*, 25–36.

Shields, A. (1936). Anwendung der Aenlichkeitsmechanik und der Turbulenzforschung auf die Geschiebebewegung. [Mitteilungen der Preussischen Versuchsanstallt fuer Wasserbau und Schiffbau, Berlin, Heft 26]. Retrieved from http://repository.tudelft.nl/view/hydro/uuid%3A61a19716-a994-4942-9906-f680eb9952d6/

Succi, S. (2001). *The lattice Boltzmann equation for fluid dynamics and beyond*. Oxford: Clarendon Press.

Ten Cate, A., Nieuwstad, C. H., Derksen, J. J., & Van den Akker, H. E. A. (2002). PIV experiments and lattice-Boltzmann simulations on a single sphere settling under gravity. *Physics of Fluids*, *14*, 4012–4024.

Uijttewaal, W. S. J. (2014). Hydrodynamics of shallow flows: application to rivers. *Journal of Hydraulic Research*, *52*, 157–172.

Vollmer, S., & Kleinhans, M. G. (2007). Predicting incipient motion, including the effect of turbulent pressure fluctuations in the bed. *Water Resources Research*, *45*, W05410-1-16.

Vowinckel, B., Kempe, T., & Fröhlich, J. (2014). Fluid–particle interaction in turbulent open channel flow with fully-resolved mobile beds. *Advances in Water Resources*, *72*, 32–44.

Yamamoto, Y., Potthoff, M., Tanaka, T., Kajishima, T., & Tsuji, Y. (2001). Large-eddy simulation of turbulent gas-particle flow in a vertical channel: effect of considering inter-particle collisions. *Journal of Fluid Mechanics*, *442*, 303–334.